

A Numerical Investigation for a Model of the Solid-Gas Phase in a Crystal Growth Apparatus

Jürgen Geiser*

*Humboldt-Universität zu Berlin, Department of Mathematics Unter den Linden 6,
D-10099 Berlin, Germany.*

Received 22 December 2006; Accepted (in revised version) 6 September 2007

Available online 11 December 2007

Abstract. We present discretization and solver methods for a model of the solid-gas phase in a crystal growth apparatus. The model equations are coupled Eulerian and heat-transfer equations with flux boundary conditions. For a more detailed discussion we consider simpler equations and present time- and space-decomposition methods as solver methods to decouple the multi-physics processes. We present the error analysis for the discretization and solver methods. Numerical experiments are performed for the Eulerian and heat-transfer equation using decomposition methods. We present a real-life application of a crystal growth apparatus, based on underlying stationary heat conduction. Finally we discuss further error analysis and application to a more complex model of crystal growth.

AMS subject classifications: 74S10, 80A20, 47F05, 65M60, 80M25, 49M27

PACS: 02.60.Cb, 02.60.-x, 44.05.+e, 47.10.ab, 47.11.Df, 47.11.St, 47.27.te

Key words: Decomposition methods, finite-volume discretization, error analysis, heat equation, crystal growth.

1 Introduction

The modelling and numerical simulation of the solid-gas phase in complex apparatuses have become interesting tools for the improved design and optimization of numerous industrial processes such as crystal growth, for example by the physical vapour transport (PVT) method [25]. Because of the complex processes, a careful study is important for the correct design of numerical simulations [36]. The combination of discretization and solver methods is therefore an important task. We propose decomposition methods to break down complicated multi-physics into simpler physics. Time decomposition

*Corresponding author. *Email address:* geiser@mathematik.hu-berlin.de (J. Geiser)

methods, and their extended versions with more stable behaviour, are based on operator-splitting methods [14]. With these methods a useful decoupling of the time-scales is possible and the solvers can be applied on these different time-scales. Space decomposition methods are based on Schwarz waveform relaxation methods and their accurate error estimates [10]. These methods decouple into domains with the same equation parameters. Therefore effective spatial discretization and solver methods are applicable.

The paper is organized as follows: The mathematical model is stated in Section 2, the space discretization methods are performed with finite volume discretization and are described in Section 3. The time-discretization and decomposition methods are described in Sections 4 and 5. In Section 6 we describe the numerical experiments in which we verify our decomposition methods and simulate a realistic crystal-growth apparatus. Future work and the Conclusions are presented in Section 7.

2 Mathematical model

The motivation for this study comes from the technical demand to simulate a crystal growth apparatus for single SiC crystals. The single crystals are highly valued materials for opto-electronics and electronics [34]. The silicon carbide (SiC) bulk single crystal is produced by a growth process through physical vapour transport (PVT), called the modified Lely method. The modelling of the thermal processes within the growth apparatus is done by [26] and [37]. The underlying equations of the model are as follows:

a.) In this work, we assume that the temperature evolution inside the gas region Ω_g can be approximated by considering the gas to be pure argon. The reduced heat equation is

$$\rho_g \partial_t U_g - \nabla \cdot (\kappa_g \nabla T) = 0, \quad (2.1)$$

$$U_g = z_{Ar} R_{Ar} T, \quad (2.2)$$

where T is the temperature, t is the time, and U_g is the internal energy of the argon gas. The density of the argon gas is ρ_g , κ_g denotes the thermal conductivity, z_{Ar} is the configuration number, and R_{Ar} is the gas constant for argon.

b.) The temperature evolution inside the region of solid materials Ω_s , for example inside the silicon carbide crystal, the silicon carbide powder, the graphite, and the graphite insulation, is described by the heat equation

$$\rho_s \partial_t U_s - \nabla \cdot (\kappa_s \nabla T) = f, \quad (2.3)$$

$$U_s = \int_0^T c_s(S) dS, \quad (2.4)$$

where ρ_s is the density of the solid material, U_s is the internal energy, κ_s is the thermal conductivity, and c_s is the specific heat. Here, f represents the heat source in the material Ω_s .

These equations hold in the domains of the respective materials and are coupled by interface conditions, requiring for example the continuity of temperature and the normal components of the heat flux on the interfaces between opaque solid materials. At the interface between the solid material and the gas domain, we consider the interface condition

$$\kappa_g \nabla T \cdot \mathbf{n}_g + R - J = \kappa_s \nabla T \cdot \mathbf{n}_g, \quad (2.5)$$

where \mathbf{n}_g is the normal to the gas domain, R is the radiosity, and J is the irradiosity. The irradiosity is determined by integrating R along the whole boundary of the gas domain [26]. Moreover, we have

$$R = E + J_{\text{ref}}, \quad (2.6)$$

$$E = \sigma \epsilon T^4 \quad (\text{Stefan-Boltzmann equation}), \quad (2.7)$$

$$J_{\text{ref}} = (1 - \epsilon) J, \quad (2.8)$$

where E is the radiation, J_{ref} is the reflected radiation, ϵ is the emissivity, and σ is the Boltzmann radiation constant.

In the next section, we focus on decoupling the complicated process into simpler processes. We discretize and solve the simpler equations by more accurate methods with embedded analytical solutions [19,20].

3 Space discretization

We discuss finite volume methods as conservation-preserving methods for the balance equations.

3.1 Discretization with finite volume methods

Finite volume methods are robust discretization methods for conservative problems, see [12]. Because of the different material behaviours in the apparatus, for example the anisotropy of thermal conductivity, the underlying discretization method must be flexible to respect such modifications. The finite volume methods are predestinated for such applications, because they can be applied to unstructured grids and also material behaviours can be found in their geometries, see [12].

There exist standard techniques including the finite element method [9] (used in [11]) and the finite volume method [12] to treat such problems. The extension of such standard methods to materials with anisotropic thermal conductivity can be straightforward for simple geometries (for example if the geometry admits a discretization into a structured grid of rectangles or parallel planes). Anisotropic materials within complex geometries are typical in industrial applications. For two-dimensional domains, we apply adapted finite volume methods as described in e.g., [1,2,6,12,13].

We apply a constrained Delaunay triangulation to discretize polyhedral domains, followed by a Voronoi construction to define finite volumes. This is a well-known procedure (see [16, Sec. 3.2] and references therein). Here, we briefly review some definitions and properties that will subsequently be used in the formulation of the finite volume scheme for the anisotropic case.

An admissible discretization of material domain Ω_m , $m \in M$, consists of a finite family $\Sigma_m := (\sigma_{m,i})_{i \in I_m}$ of subsets of Ω_m satisfying a number of assumptions, subsequently denoted by (DA-*).

For $d \in \{1,2\}$, we have λ_d and denote a d -dimensional Lebesgue measure. In the following we have the notation of our finite volume method.

- (DA-1) For each $m \in M$, $\Sigma_m = (\sigma_{m,i})_{i \in I_m}$ forms a finite conforming triangulation of Ω_m . In particular, for each $i \in I_m$, $\sigma_{m,i}$ is an open triangle. Moreover, letting $I := \bigcup_{m \in M} I_m$, $\Sigma := (\sigma_i)_{i \in I}$ forms a conforming triangulation of Ω .
- (DA-2) For each $m \in M$, the triangulation $\Sigma_m = (\sigma_{m,i})_{i \in I_m}$ respects Γ_{Dir} and Γ_{Rob} in the sense that, for each $i \in I_m$, either $\lambda_1(\Gamma_{\text{Dir}} \cap \partial \sigma_{m,i}) = 0$ or $\lambda_1(\Gamma_{\text{Rob}} \cap \partial \sigma_{m,i}) = 0$.
- (DA-3) For each $m \in M$, the triangulation Σ_m has the constrained Delaunay property: If $\tilde{V}_m := \bigcup_{i \in I_m} V(\sigma_{m,i})$, then for each $(v,z) \in \tilde{V}_m^2$ such that $v \neq z$, the following conditions (a) and (b) are satisfied:
 - (a) If the boundaries of the Voronoi cells corresponding to v and z have a one-dimensional intersection, i.e. if $\lambda_1(\partial \omega_{m,v} \cap \partial \omega_{m,z}) \neq \emptyset$, then $[v,z]$ is an edge of at least one $\sigma \in \Sigma_m$.
 - (b) If $[v,z]$ is an edge of at least one $\sigma \in \Sigma_m$, then the boundaries of the corresponding Voronoi cells have a nonempty intersection, i.e., $\partial \omega_{m,v} \cap \partial \omega_{m,z} \neq \emptyset$.

For each $\sigma_{m,i}$, let $V(\sigma_{m,i}) = \{v_{i,j}^m : j \in \{1,2,3\}\}$ denote the set of vertices of $\sigma_{m,i}$, and let $V := \bigcup_{m \in M, i \in I_m} V(\sigma_{m,i})$ be the set of all vertices in the triangulation. One can then define the control volumes as the Voronoi cells with respect to the vertices. Using $\|\cdot\|_2$ to denote Euclidean distance, we define

$$\begin{aligned} \text{for all } v \in V: \omega_v &:= \{x \in \Omega : \|x-v\|_2 < \|x-z\|_2 \text{ for each } z \in V \setminus \{v\}\}, \\ \text{for all } m \in M: \omega_{m,v} &:= \omega_v \cap \Omega_m, \quad V_m := \{z \in V : \omega_{m,z} \neq \emptyset\}. \end{aligned}$$

Letting $\mathcal{T} := (\omega_v)_{v \in V}$, $\mathcal{T}_m := (\omega_{m,v})_{v \in V_m}$, $m \in M$, \mathcal{T} forms a partition of Ω , and \mathcal{T}_m forms a partition of Ω_m .

Remark 3.1. Due to the two-dimensional setting, (DA-3) can be expressed equivalently in terms of the angles in the triangulation: For each $m \in M$, if γ is an interior edge of the triangulation Σ_m , and α and β are the angles opposite to γ , then $\alpha + \beta \leq \pi$. If $\gamma \subseteq \partial \Omega_m$ is a boundary edge of Σ_m , and α is the angle opposite γ , then $\alpha \leq \pi/2$.

The following remark allows the incorporation of the interface condition (2.5) into the finite volume scheme.

Remark 3.2. Using our finite volume notation, we can show that (DA-1) and (DA-3) imply the following assertions (a) and (b):

- (a) For each $m \in M$, the set V_m defined above is identical to the set \tilde{V}_m defined in (DA-3).
- (b) Let Γ be a one-dimensional material interface: $\Gamma = \partial\Omega_m \cap \partial\Omega_{\tilde{m}}$, $\lambda_1(\Gamma) \neq 0$. For each $v \in V$, if some $\bar{\omega}_v$ has a one-dimensional intersection with the interface Γ , then it lies on both sides of the intersection; in other words, $\partial_{\text{reg}}\omega_{m,v} \cap \Gamma = \partial_{\text{reg}}\omega_{\tilde{m},v} \cap \Gamma$, in particular, $\lambda_1(\partial\omega_{m,v} \cap \Gamma) \neq 0$ if and only if $\lambda_1(\partial\omega_{\tilde{m},v} \cap \Gamma) \neq 0$.

Integrating (2.3) over $\omega_{m,v}$ and applying the Gauss-Green integration theorem yields

$$\int_{\omega_{m,v}} \rho_s \partial_t u_s dx - \int_{\partial\omega_{m,v}} (K_m(\tau) \nabla \tau) \bullet \mathbf{n}_{\omega_{m,v}} dx = \int_{\omega_{m,v}} f_m dx, \tag{3.2}$$

where $\mathbf{n}_{\omega_{m,v}}$ denotes the outer unit normal vector to $\omega_{m,v}$. $f_m \geq 0$ represent the heat source in material m , Ω_m is the domain of material m , and M is a finite index set.

4 Time discretization

For the time discretization of the parabolic equations, we propose the standard Runge-Kutta methods and BDF methods [23]. These methods are stable and simple to implement.

For the combination with our operator-splitting, we propose high order methods, that will fit best for each time-scale. Because of the decoupling, each resulting equation has to be treated with the appropriate time-step and the standard time discretization method of high order.

An important class of time-discretization methods are the IMEX (implicit-explicit) methods. These are a combination of mixed discretization methods for stiff operators (implicit method) and non-stiff operators (explicit method) [3]. Because of the combination of two discretization methods, the methods are more time consuming and we do not apply them.

For our iterative splitting methods, we apply standard time-discretization methods of high order, that are less time consuming. The delicate initialization process with the initial solution at the first iteration step can be overcome with high order discretization [14]. For the next iteration step the order has to be increased till the proposed order of the time discretization is reached. We deal therefore with the following two methods, that fit our splitting methods.

4.1 Runge-Kutta method

The Runge-Kutta methods are known to be one-step methods for ODEs and obtain sufficiently high order accuracy and stability [7]. Because of the order reduction, which shows up in high accuracy calculations of initial boundary value problems, we propose to use the method in the initialization process of our splitting methods or for less stiff problems [23].

We use the following two RK-methods: The implicit trapezoidal rule, which is given by

$$\begin{array}{c|cc} 0 & & \\ 1 & \frac{1}{2} & \frac{1}{2} \\ \hline & \frac{1}{2} & \frac{1}{2} \end{array}, \quad (4.1)$$

and the Gauß Runge-Kutta method which is given by

$$\begin{array}{c|cc} \frac{1}{2} - \frac{\sqrt{3}}{6} & \frac{1}{4} & \frac{1}{4} - \frac{\sqrt{3}}{6} \\ \frac{1}{2} + \frac{\sqrt{3}}{6} & \frac{1}{4} + \frac{\sqrt{3}}{6} & \frac{1}{4} \\ \hline & \frac{1}{2} & \frac{1}{2} \end{array}. \quad (4.2)$$

To use these Runge-Kutta methods with our operator-splitting method we have to take into account that we solve equations of the form

$$\frac{\partial u_i}{\partial t} = Au_i + b$$

for each iteration, where $b = Bu_{i-1}$ is a discrete function, as we have only a discrete solution for u_{i-1} .

For the implicit trapezoidal rule this is no problem, because we do not need the values at any sub-points. On the other hand, for the Gauß method we need to know the values of b at the sub-points $t_0 + c_1h$ and $t_0 + c_2h$ with $c = (\frac{1}{2} - \frac{\sqrt{3}}{6}, \frac{1}{2} + \frac{\sqrt{3}}{6})^T$. Therefore we must interpolate b . To do so we choose cubic spline functions. Numerical experiments show that this works properly with non-stiff problems, but not with stiff-problems.

4.2 BDF method

Their robustness and stability for stiff problems [7,23], and their simpler implementation with respect to the implicit method, motivates our use of BDF methods.

Initial experiments, based on the high order Gauß Runge-Kutta method in combination with cubic spline interpolation, did not work properly with stiff problems. Therefore, we use the following BDF method and of order at least three, which does not require sub-points and therefore no interpolation is needed. The BDF3 method is given by

$$\frac{1}{k} \left(\frac{11}{6} u^{n+2} - 3u^{n+1} + \frac{3}{2} u^n - \frac{1}{3} u^{n-1} \right) = A(u^{n+3}). \quad (4.3)$$

To compute the pre-steps u^n and u^{n-1} , for example the first results u_1, u_2 , we use the implicit trapezoidal rule of second order.

The application of the BDF3 methods to our operator-splitting method is more straightforward. We take the iteration equations of the form $\partial_t u_i = Au_i + b$, where $b = Bu_{i-1}$ is a discrete function, for the right-hand side. The computation of the second equation requires only a simple change of the iterative equations to $\partial_t u_{i+1} = Bu_{i+1} + b$, where $b = Au_i$ is the right-hand side, known from the previous iterative solution. There is no need to compute intermediate time-steps, which is an enormous computational benefit [7]. Decomposition methods are explained in the next section.

5 Decomposition methods

In this section, we describe the underlying time and spatial decomposition methods used to reduce the complexity of the given equation [21].

5.1 Time-decomposition methods: Operator-splitting

Operator-splitting methods are used to solve complex models in the geophysical and environmental physics. They are developed and applied in [42, 43]. We apply our contributed ideas to decouple complicate systems of differential equations in simpler systems of differential equations. These resulting equations can be solved with standard higher order methods, see [21]. For this we use the operator-splitting method and decouple the equation as follows.

5.1.1 First order Splitting methods for linear equations

First we describe the simplest operator-splitting, known as A - B or sequential splitting, for the following system of ordinary linear differential equations:

$$\frac{\partial c(t)}{\partial t} = Ac(t) + Bc(t), \quad (5.1)$$

where the initial-conditions are $c^n = c(t^n)$. The operators A and B are spatially discretized operators. They might for example correspond to the spatially discretize convection and diffusion operators (matrices). They can therefore be considered as bounded operators.

The sequential operator-splitting method is a method for solving two sub-problems sequentially, where the different sub-problems are connected via the initial conditions. This means that we replace the original problem (5.1) with the sub-problems

$$\begin{aligned} \frac{\partial c^*(t)}{\partial t} &= Ac^*(t), & \text{with } c^*(t^n) &= c^n, \\ \frac{\partial c^{**}(t)}{\partial t} &= Bc^{**}(t), & \text{with } c^{**}(t^n) &= c^*(t^{n+1}), \end{aligned} \quad (5.2)$$

where the splitting time-step is defined as $\tau_n = t^{n+1} - t^n$. The approximated split solution is defined as

$$c^{n+1} = c^{**}(t^{n+1}).$$

Clearly, the replacement of the original problems with the sub-problems usually results in some error, called the *splitting error*. The splitting error of the sequential splitting method can be derived as follows

$$\begin{aligned} \rho_n &= \frac{1}{\tau} \left(\exp(\tau_n(A+B)) - \exp(\tau_n B) \exp(\tau_n A) \right) c(t^n) \\ &= \frac{1}{2} \tau_n [A, B] c(t^n) + \mathcal{O}(\tau^2). \end{aligned} \quad (5.3)$$

where $[A, B] := AB - BA$ is the commutator of A and B . Consequently, the splitting error is $\mathcal{O}(\tau_n)$ when the operators A and B do not commute, otherwise the method is exact. Therefore sequential splitting is also known as the *first order splitting method*.

5.1.2 Iterative splitting method

The following algorithm is based on iteration with a fixed splitting discretization step-size τ . On the time interval $[t^n, t^{n+1}]$ we solve the following sub-problems consecutively for $i = 0, 2, \dots, 2m$ (see, e.g., [14, 24]):

$$\frac{\partial c_i(t)}{\partial t} = Ac_i(t) + Bc_{i-1}(t), \quad \text{with } c_i(t^n) = c^n, \quad (5.4)$$

$$\frac{\partial c_{i+1}(t)}{\partial t} = Ac_i(t) + Bc_{i+1}(t), \quad \text{with } c_{i+1}(t^n) = c^n, \quad (5.5)$$

where $c_0(t^n) = c^n$, $c_{-1} = 0$, c^n is the known split approximation at the time level $t = t^n$. The split approximation at the time level $t = t^{n+1}$ is defined as

$$c^{n+1} = c_{2m+1}(t^{n+1}).$$

Clearly, the function $c_{i+1}(t)$ depends on the interval $[t^n, t^{n+1}]$ too, but for the sake of simplicity, in our notation we omit the dependence on n .

In the following, we will present the convergence and the rate of convergence of the method (5.4)-(5.5) for the linear operators $A, B: \mathbf{X} \rightarrow \mathbf{X}$ where we assume that these operators and their sum are generators of the C_0 semi groups. We emphasize that these operators are not necessarily bounded, so the convergence is examined in a general Banach space setting. The following result was proven in [14].

Theorem 5.1. *Let us consider the abstract Cauchy problem in a Banach space \mathbf{X} :*

$$\begin{aligned} \frac{\partial c(t)}{\partial t} &= Ac(t) + Bc(t), \quad 0 < t \leq T, \\ c(0) &= c_0, \end{aligned} \quad (5.6)$$

where $A, B, A+B: \mathbf{X} \rightarrow \mathbf{X}$ are given linear operators being generators of the C_0 -semigroup and $c_0 \in \mathbf{X}$ is a given element. Then the iteration process (5.4)-(5.5) is convergent and the rate of the convergence is of second order.

Remark 5.1. When A and B are matrices (i.e. (5.4)-(5.5) is a system of ordinary differential equations), we can use the concept of the logarithmic norm to estimate the growth (see, e.g., [23]). Hence, for many important classes of matrices we can prove the validity of this theorem.

Remark 5.2. We note that a large class of important differential operators generate contractive semigroups. This means that for such problems – assuming the exact solvability of the split sub-problems – the iterative splitting method is convergent in second order to the exact solution.

5.2 Domain decomposition methods: Schwarz waveform relaxation

In this subsection we show that the overlapping Schwarz waveform relaxation method is a flexible decomposition method for multi-domain applications such as those presented in Subsection 6.3.

We present the method and the convergence analysis for a convection-diffusion-reaction equation, and also for heat equations. The method can be extended to multiple dimensions and parabolic equation systems [10].

We consider the convection-diffusion-reaction equation:

$$u_t = Du_{xx} - vu_x - \lambda u, \tag{5.7}$$

defined in the domain $\Omega = [0, L]$ for $T = [T_0, T_f]$, with the following initial and boundary conditions

$$u(0, t) = f_1(t), \quad u(L, t) = f_2(t), \quad u(x, T_0) = u_0.$$

To solve the model problem using the overlapping Schwarz waveform relaxation method, we subdivide the domain Ω in two overlapping sub-domains $\Omega_1 = [0, L_2]$ and $\Omega_2 = [L_1, L]$, where $L_1 < L_2$ and $\Omega_1 \cap \Omega_2 = [L_1, L_2]$ is the overlapping region for Ω_1 and Ω_2 .

To begin the waveform relaxation algorithm we first consider the solution of the model problem (5.7) over Ω_1 as follows

$$\begin{aligned} v_t &= Dv_{xx} - vv_x - \lambda v, & x \in \Omega_1, & t \in [T_0, T_f], \\ v(0, t) &= f_1(t), & v(L_2, t) &= w(L_2, t), & t \in [T_0, T_f], \\ v(x, T_0) &= u_0, & x \in \Omega_1; \end{aligned} \tag{5.8}$$

and

$$\begin{aligned} w_t &= Dw_{xx} - vw_x - \lambda w, & x \in \Omega_2, & t \in [T_0, T_f], \\ w(L_1, t) &= v(L_1, t), & w(L, t) &= f_2(t), & t \in [T_0, T_f], \\ w(x, T_0) &= u_0, & x \in \Omega_2, \end{aligned} \tag{5.9}$$

where $v(x,t)=u(x,t)|_{\Omega_1}$ and $w(x,t)=u(x,t)|_{\Omega_2}$. The Schwarz waveform relaxation is then given by

$$\begin{aligned} v_t^{k+1} &= Dv_{xx}^{k+1} - v v_x^{k+1} - \lambda v^{k+1}, & x \in \Omega_1, & t \in [T_0, T_f], \\ v^{k+1}(0,t) &= f_1(t), & v^{k+1}(L_2,t) &= w^k(L_2,t), & t \in [T_0, T_f], \\ v^{k+1}(x, T_0) &= u_0, & x \in \Omega_1, \end{aligned} \tag{5.10}$$

and

$$\begin{aligned} w_t^{k+1} &= Dw_{xx}^{k+1} - v w_x^{k+1} - \lambda w^{k+1}, & x \in \Omega_2, & t \in [T_0, T_f], \\ w^{k+1}(L_1,t) &= v^k(L_1,t), & w^{k+1}(L,t) &= f_2(t), & t \in [T_0, T_f], \\ w^{k+1}(x, T_0) &= u_0, & x \in \Omega_2. \end{aligned} \tag{5.11}$$

We are interested in estimating the decay of the error in the over the overlapping sub-domains in the solution found by the overlapping Schwarz waveform relaxation method over a long time interval.

Let us assume that $e^{k+1}(x,t) = u(x,t) - v^{k+1}(x,t)$ and $d^{k+1}(x,t) = u(x,t) - w^{k+1}(x,t)$ are the errors of (5.10) and (5.11) over Ω_1 and Ω_2 , respectively. The corresponding differential equations satisfied by $e^{k+1}(x,t)$ and $d^{k+1}(x,t)$ are

$$\begin{aligned} e_t^{k+1} &= De_{xx}^{k+1} - v e_x^{k+1} - \lambda e^{k+1}, & x \in \Omega_1, & t \in [T_0, T_f], \\ e^{k+1}(0,t) &= 0, & e^{k+1}(L_2,t) &= d^k(L_2,t), & t \in [T_0, T_f], \\ e^{k+1}(x, T_0) &= 0, & x \in \Omega_1, \end{aligned} \tag{5.12}$$

and

$$\begin{aligned} d_t^{k+1} &= Dd_{xx}^{k+1} - v d_x^{k+1} - \lambda d^{k+1}, & x \in \Omega_2, & t \in [T_0, T_f], \\ d^{k+1}(L_1,t) &= e^k(L_1,t), & d^{k+1}(L,t) &= 0, & t \in [T_0, T_f], \\ d^{k+1}(x, T_0) &= 0, & x \in \Omega_2. \end{aligned} \tag{5.13}$$

We define, for bounded functions $h(x,t) : \Omega \times [T_0, T] \rightarrow \mathbf{R}$, the norm

$$\|h(\cdot, \cdot)\|_\infty := \sup_{x \in \Omega, t \in [T_0, T_f]} |h(x,t)|.$$

The theory behind our error estimates is based on the positivity lemma by Pao (or the maximum principle theorem) [35].

The convergence and error estimates of e^{k+1} and d^{k+1} given by (5.12)-(5.13) are summarized below and were proved in [10].

Theorem 5.2. *Let e^{k+1} and d^{k+1} be the errors from the solution of the sub-problems (5.12)-(5.13) by Schwarz waveform relaxation over Ω_1 and Ω_2 respectively. Then*

$$\|e^{k+2}(L_1,t)\|_\infty \leq \gamma \|e^k(L_1,t)\|_\infty, \tag{5.14}$$

$$\|d^{k+2}(L_2,t)\|_\infty \leq \gamma \|d^k(L_1,t)\|_\infty, \tag{5.15}$$

where

$$\gamma = \frac{\sinh(\beta L_1) \sinh(\beta(L_2 - L))}{\sinh(\beta L_2) \sinh(\beta(L_1 - L))} < 1, \quad \beta = \frac{\sqrt{v^2 + 4D\lambda}}{2D}. \tag{5.16}$$

Theorem 5.2 shows that the convergence of the overlapping Schwarz method depends on γ defined by (5.16). Due to the characteristic of the sinh function we will have a sharp decay of the error for any $L_1 < L_2$, or for a large degree of overlap.

We have applied this method for the convection-diffusion-reaction equation. For the heat equation we can apply Theorem 5.2 with the parameter $\nu = \lambda = 0$. In the next section we present numerical results.

6 Numerical results

In this section we present numerical experiments with two test examples and a real-life application. We verify the decomposition methods with test examples for the convection-reaction and heat equations. Based on these results we present a real-life application. We discuss the heat equation in different material layers and outline a more efficient treatment based on decomposition methods.

6.1 Convection-reaction equation for a mixture of gasses

We apply operator-splitting methods for the convection-reaction equation. Our underlying transport equation is given by

$$\partial_t u_1 = -v_1 \partial_x u_1 - \lambda u_1, \tag{6.1}$$

$$\partial_t u_2 = -v_2 \partial_x u_2 + \lambda u_1, \tag{6.2}$$

with the initial and boundary conditions

$$u_1(x,0) = \begin{cases} 1, & \text{for } 0.1 \leq x \leq 0.3, \\ 0, & \text{otherwise,} \end{cases} \tag{6.3}$$

$$u_2(x,0) = 0, \quad \text{for } x \in [0, X], \tag{6.4}$$

$$u_1(0,t) = u_2(0,t) = 0, \quad \text{for } t \in [0, T], \tag{6.5}$$

where $\lambda \in \mathcal{R}^+$ and $v_1, v_2 \in \mathcal{R}^+$. We have the time interval $t \in [0, T]$ and the space interval $x \in [0, X]$. We apply the equations with $X=1.5$ and $T=1.0$. We rewrite the equation system (6.1)-(6.5) in operator notation, and obtain the following equations:

$$\partial_t u = Au + Bu, \tag{6.6}$$

$$u(x,0) = \begin{cases} (1,0)^T, & \text{for } 0.1 \leq x \leq 0.3, \\ (0,0)^T, & \text{otherwise,} \end{cases} \tag{6.7}$$

where $u = (u_1, u_2)^T$. Our split operators are

$$A = \begin{pmatrix} -v_1 \partial_x & 0 \\ 0 & -v_2 \partial_x \end{pmatrix}, \quad B = \begin{pmatrix} -\lambda & 0 \\ \lambda & 0 \end{pmatrix}. \tag{6.8}$$

We use the finite-difference method for spatial discretization and solve the time discretization analytically.

The spatial discretization is done as follows. We concentrate on the interval $x \in [0, 1.5]$ and we consider a uniform partition thereof with step-size $\Delta x = 0.1$. For the transport term we use an upwind finite-difference discretization given by:

$$\partial_x u_i = \frac{u_i - u_{i-1}}{\Delta x}. \quad (6.9)$$

We use for the initial values, the following impuls function is given:

$$u_1(x) = \begin{cases} 1, & 0.1 \leq x \leq 0.3, \\ 0, & \text{otherwise,} \end{cases} \quad (6.10)$$

$$u_2(x) = 0, \quad x \in [0, 1.5]. \quad (6.11)$$

For the iterative operator-splitting method and its application to our transport equation we use the discretized equation with two indices. Index i is used for the spatial discretization and the index j is used for the iterations.

We first solve all the equations with the index i , that is all sixteen equations for each point. Then we perform our iterations and obtain the first time-step. The process is then complete for one time partition. We repeat this four times for the computation of five partitions and so on.

In the following equations we write the iterative operator-splitting algorithm by taking into account the discretization in space. The time discretization is solved analytically. We solve the following problems consecutively for $j = 1, 3, 5, \dots$ for the time interval $[t^n, t^{n+1}]$. The split approximation at the time level $t = t^{n+1}$ is defined as $u_i^{n+1} \equiv u_{i,iter}(t^{n+1})$.

We then have the following algorithm:

$$\partial_t u_{1,i,j} = -v_1 / \Delta x (u_{1,i,j} - u_{1,i-1,j}) - \lambda u_{1,i,j-1}, \quad (6.12)$$

$$\partial_t u_{2,i,j} = -v_2 / \Delta x (u_{2,i,j} - u_{2,i-1,j}) + \lambda u_{1,i,j-1}, \quad (6.13)$$

$$\partial_t u_{1,i,j+1} = -v_1 / \Delta x (u_{1,i,j} - u_{1,i-1,j}) - \lambda u_{1,i,j+1}, \quad (6.14)$$

$$\partial_t u_{2,i,j+1} = -v_2 / \Delta x (u_{2,i,j} - u_{2,i-1,j}) + \lambda u_{1,i,j+1}, \quad (6.15)$$

with the initial conditions

$$u_{1,i,j}(0) = \begin{cases} 1, & \text{for } i = 1, 2, 3, \\ 0, & \text{otherwise,} \end{cases} \quad (6.16)$$

$$u_{2,i,j}(0) = 0, \quad \text{for } i = 0, \dots, 15, \quad (6.17)$$

where $\lambda = 0.5$ and $v_1 = 0.5$ and $v_2 = 1.0$. For the time interval we use $t \in [0, 1]$. The analytical solution of the equation system (6.1)-(6.5) is

$$u_1(x, t) = \begin{cases} \exp(-\lambda t), & \text{for } 0.1 + v_1 t \leq x \leq 0.3 + v_1 t, \\ 0, & \text{otherwise,} \end{cases}$$

$$u_2(x, t) = \lambda (L_{1,2} + L_{2,2} + M_{12,2}).$$

In the following, the factors $L_{1,2}$, $L_{2,2}$ and $M_{12,2}$ are given by

$$L_{1,2} = \begin{cases} -\frac{1}{\lambda} \exp(-\lambda t), & \text{for } 0.1 + v_1 t \leq x \leq 0.3 + v_1 t, \\ 0, & \text{otherwise,} \end{cases}$$

$$L_{2,2} = \begin{cases} \frac{1}{\lambda}, & \text{for } 0.1 + v_2 t \leq x \leq 0.3 + v_2 t, \\ 0, & \text{otherwise,} \end{cases}$$

and

$$M_{12,2} = \begin{cases} \frac{1}{\lambda} \exp(-\lambda t) \\ \exp(-(\frac{\lambda}{v_1 - v_2})(x - v_1 t - 0.1)), & \text{for } 0.1 + v_1 t \leq x \leq 0.1 + v_2 t \\ -\frac{1}{\lambda} \exp(-\lambda t) \\ \exp(-(\frac{\lambda}{v_1 - v_2})(x - v_1 t - 0.3)), & \text{for } 0.3 + v_1 t \leq x \leq 0.3 + v_2 t, \\ 0, & \text{otherwise.} \end{cases}$$

So, at the end time $t_{end} = 1$, we check the results for the endpoint $x_1 = v_1 t + 0.3$. We get the exact solution:

$$u_1(x_1, t_{end}) = 0.60653, \quad u_2(x_1, t_{end}) = 0.$$

In Table 1 we give the errors for the exact solutions at the end time $t = 1$ and endpoint $x = v_1 t + 0.3 = 0.8$. The experiments were performed in Matlab 7.0 with a Linux Personal Computer (PC), 2 GHz with computation accuracy of about 10^{-313} .

Table 1: Numerical results for the first example with the iterative splitting method.

Number of time partitions	Iterative Steps	err_1	err_2
1	2	2.679116×10^{-1}	2.465165×10^{-1}
1	4	1.699365×10^{-1}	3.584424×10^{-1}
1	10	2.702681×10^{-1}	5.327567×10^{-2}
1	50	6.065295×10^{-1}	6.170954×10^{-7}
1	100	6.065307×10^{-1}	7.152770×10^{-17}
5	2	2.472959×10^0	6.812055×10^{-1}
5	4	1.181408×10^1	4.757047×10^0
5	10	4.680711×10^0	1.496981×10^0
5	50	8.208500×10^{-2}	7.325327×10^{-25}
5	100	8.208500×10^{-2}	1.299116×10^{-70}
10	2	2.289850×10^2	7.246663×10^1
10	4	1.121958×10^4	4.498364×10^3
10	10	8.999232×10^4	2.819985×10^4
10	50	6.737947×10^{-3}	2.593585×10^{-34}
10	100	6.737947×10^{-3}	3.160841×10^{-70}

Remark 6.1. The benefit of the iterative operator-splitting method can be seen in the optimal choice of time-steps and iterations. According to our results, smaller time-steps

are expensive, because the repetition of many linear solver steps are required. But with further iterations combined with larger time-steps we can achieve more accurate results with less time-consuming methods. Therefore we propose more iterations and a small number of time partitions to reach the optimal results.

6.2 Heat equation with nonlinear heat source

In the second test example we examine a two-dimensional heat equation with a nonlinear heat source [3]:

$$\partial_t u(x,y,t) = u_{xx} + u_{yy} - 4(1+y^2)e^{-t}e^{x+y^2}, \quad (6.18)$$

$$u(x,y,0) = e^{x+y^2} \text{ in } \Omega = [-1,1] \times [-1,1], \quad (6.19)$$

$$u(x,y,t) = e^{-t}e^{x+y^2} \text{ on } \partial\Omega, \quad (6.20)$$

with the exact solution

$$u(x,y,t) = e^{-t}e^{x+y^2}. \quad (6.21)$$

We choose the time interval $[0,1]$ and again apply finite differences for this space with $\Delta x = 2/19$. We use the operator-splitting method for decomposition. The domain is split into two sub-domains. The operator equation is given by

$$\partial_t u(x,y,t) = Au + Bu + f(x,y),$$

where

$$f(x,y) = -4(1+y^2)e^{-t}e^{x+y^2},$$

and the operators are given by

$$Au = \begin{cases} u_{xx} + u_{yy} & \text{for } (x,y) \in \Omega_1, \\ 0 & \text{for } (x,y) \in \Omega_2, \end{cases} \quad (6.22)$$

$$Bu = \begin{cases} 0 & \text{for } (x,y) \in \Omega_1, \\ u_{xx} + u_{yy} & \text{for } (x,y) \in \Omega_2, \end{cases} \quad (6.23)$$

where $\Omega_1 \cup \Omega_2 = \Omega$ and $\Omega_1 \cap \Omega_2 = \emptyset$. The initial and boundary conditions are given by equations (6.19)-(6.20).

We choose the splitting intervals $\Omega_1 = [-1,0] \times [-1,1]$ and $\Omega_2 = [0,1] \times [-1,1]$. The maximum approximation error is given by

$$\text{Max-error} = \left| \max_{i,j} u_{exact}(x_i, y_j, T) - u_{approx}(i\Delta x, j\Delta x, T) \right|,$$

where $T = 1$.

The results of the experiment are presented in Table 2. One can see the decrease in the maximum error with respect to the number of iterations. Further comparisons to other

Table 2: Numerical results for the second example with the Iterative Operator Splitting method and BDF3 with $h = 10^{-1}$.

Iterative Steps	Number of splitting-partitions	Max-error L_∞
1	1	2.7183e+000
2	1	8.2836e+000
3	1	3.8714e+000
4	1	2.5147e+000
5	1	1.8295e+000
10	1	6.8750e-001
15	1	2.5764e-001
20	1	8.7259e-002
25	1	2.5816e-002
30	1	5.3147e-003
35	1	2.8774e-003

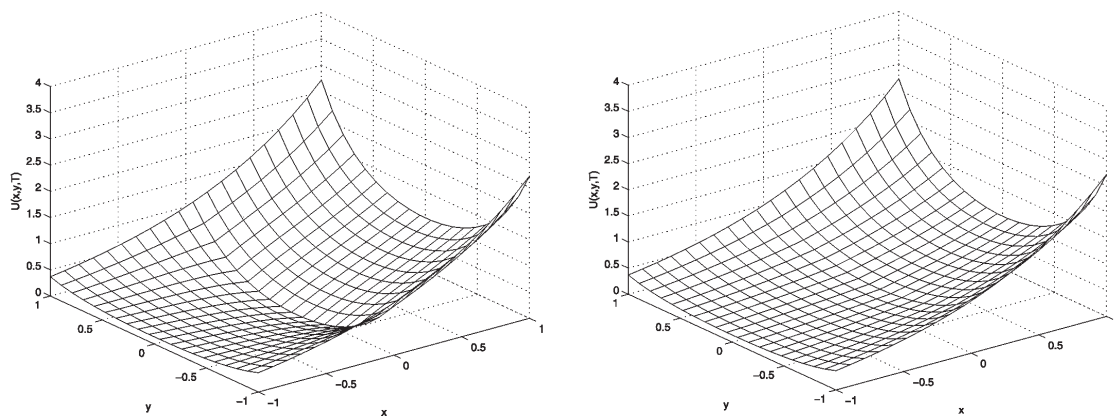


Figure 1: The numerical results of the second example after ten iterations (left) and twenty iterations (right).

methods are made in [22]. Based on these results, the iterative operator splitting-method appears more accurate.

It can be seen graphically in Fig. 1 that the solution becomes smoother with increasing numbers of relaxation steps.

Remark 6.2. Here the results of the previous experiments are used to deal with large time-steps. With the largest time-step and with about 15-20 iterations we achieve our required maximum error of about 10^{-2} . By using the splitting method we can decouple to simpler domains and reduce the amount of computational time.

6.3 Real-life problem: crystal growth apparatus

Here we examine stationary heat conduction in potentially anisotropic materials. We require the following underlying equations:

$$-\operatorname{div}(K_m(\theta)\nabla\theta) = f_m \quad \text{in } \Omega_m \quad (m \in M), \quad (6.24)$$

where $\theta \geq 0$ represents absolute temperature, the symmetric and positive definite matrix K_m represents the thermal conductivity tensor in material m , $f_m \geq 0$ represents heat sources in material m due to some heating mechanism such as induction or resistance heating, Ω_m is the domain of material m , and M is a finite index set. We consider the case where the thermal conductivity tensor is a diagonal matrix with temperature-independent anisotropy so that

$$K_m(\theta) = (\kappa_{i,j}^m(\theta)), \quad \text{where} \quad \kappa_{i,j}^m(\theta) = \begin{cases} \alpha_i^m \kappa_{\text{iso}}^m(\theta) & \text{for } i=j, \\ 0 & \text{for } i \neq j, \end{cases} \quad (6.25)$$

where $\kappa_{\text{iso}}^m(\theta) > 0$ is the potentially temperature-dependent thermal conductivity of the isotropic case, and $\alpha_i^m > 0$ are anisotropy coefficients. For example, the growth apparatus used in silicon carbide single crystal growth using PVT is usually insulated by graphite felt, where the fibres are aligned in one particular direction, resulting in a thermal conductivity tensor of the form (6.25). We apply the finite-volume scheme described in Section 3.1 and consider the anisotropy in the thermal insulation of the physical vapour transport (PVT) growth apparatus in [18].

The temperature θ is assumed to be continuous throughout the entire domain $\overline{\Omega}$. Continuity of the normal component of the heat flux on the interface between different materials m_1 and m_2 , $m_1 \neq m_2$, yields the following interface conditions, coupling the heat equations (6.24):

$$(K_{m_1}(\theta)\nabla\theta)|_{\overline{\Omega}_{m_1}} \bullet \mathbf{n}_{m_1} = (K_{m_2}(\theta)\nabla\theta)|_{\overline{\Omega}_{m_2}} \bullet \mathbf{n}_{m_1} \quad \text{on } \overline{\Omega}_{m_1} \cap \overline{\Omega}_{m_2}, \quad (6.26)$$

where $|$ denotes restriction, and \mathbf{n}_{m_1} denotes the unit normal vector pointing from material m_1 to material m_2 .

We consider two types of outer boundary condition, namely Dirichlet and Robin conditions. To that end, we decompose $\partial\Omega$ according to (A-1) thus

$$(A-1) \quad \text{Let } \Gamma_{\text{Dir}} \text{ and } \Gamma_{\text{Rob}} \text{ be relatively open polyhedral subsets of } \partial\Omega \text{ such that } \partial\Omega = \overline{\Gamma}_{\text{Dir}} \cup \overline{\Gamma}_{\text{Rob}}, \quad \Gamma_{\text{Dir}} \cup \Gamma_{\text{Rob}} = \emptyset.$$

The boundary conditions are then

$$\theta = \theta_{\text{Dir}} \quad \text{on } \overline{\Gamma}_{\text{Dir}}, \quad (6.27a)$$

$$-(K_m(\theta)\nabla\theta) \bullet \mathbf{n}_m = \zeta_m(\theta - \theta_{\text{ext},m}), \quad \text{a.e. on } \Gamma_{\text{Rob}} \cap \partial\Omega_m, \quad m \in M, \quad (6.27b)$$

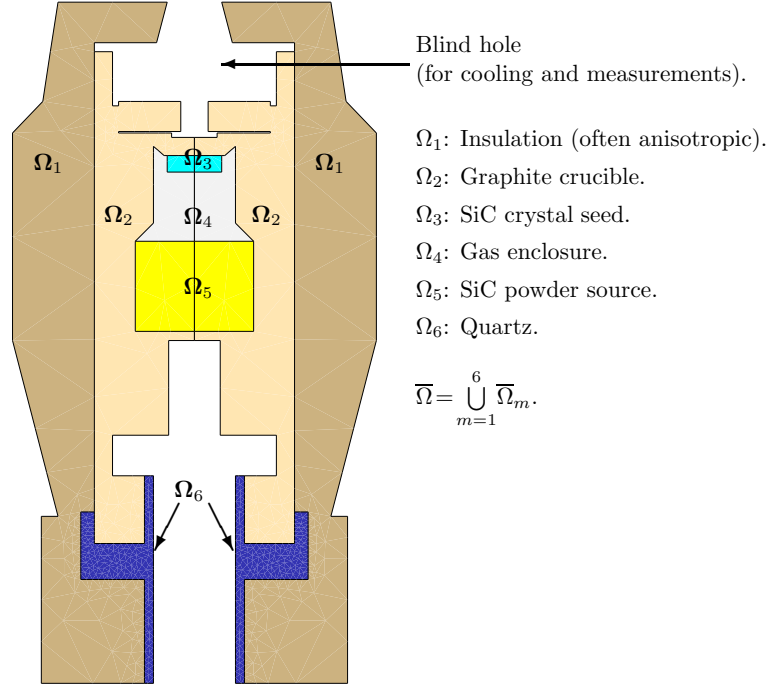


Figure 2: The modelled apparatus shown as an axisymmetric domain with regions regions of different materials.

where \mathbf{n}_m is the outer unit normal to Ω_m , $\theta_{\text{Dir}} \geq 0$ is the given temperature on Γ_{Dir} , $\theta_{\text{ext},m} \geq 0$ is the given external temperature ambient to $\Gamma_{\text{Rob}} \cap \partial\Omega_m$, and $\zeta_m > 0$ is a transition coefficient. Our geometry of the apparatus is shown in Fig. 2. The radius of the domain is 12cm and the height is 45.3cm. This represents a growth apparatus used in silicon carbide single crystal growth by the PVT method. Ω consists of six subdomains Ω_m , $m \in \{1, \dots, 6\}$, representing the insulation, graphite crucible, SiC crystal seed, gas enclosure, SiC powder source and quartz. Aiming to use realistic functions for the isotropic parts $\kappa_{\text{iso}}^m(\theta)$ of the thermal conductivity tensors (cf. (6.25)), the gas enclosure, graphite crucible, insulation and SiC crystal seed, we use the functions given by (A.1), (A.3b), (A.4b) and (A.7b) in [30]; for $\kappa_{\text{iso}}^5(\theta)$ (the SiC powder source), we use [28, (A.1)], and for $\kappa_{\text{iso}}^6(\theta)$ (quartz), we use

$$\kappa_{\text{iso}}^6(\theta) = \left(1.82 - 1.21 \cdot 10^{-3} \frac{\theta}{\text{K}} + 1.75 \cdot 10^{-6} \frac{\theta^2}{\text{K}^2} \right) \frac{\text{W}}{\text{mK}}. \quad (6.28)$$

Hence, all functions $\kappa_{\text{iso}}^m(\theta)$ depend nonlinearly on θ . As mentioned in the introduction the thermal conductivity in the insulation is typically anisotropic in PVT growth apparatus. We therefore vary the anisotropy coefficients (α_r^1, α_z^1) of the insulation while keeping $(\alpha_r^m, \alpha_z^m) = (1, 1)$ for all other materials $m \in \{2, 3, 4, 5\}$ in the numerical experiments described below.

Heat sources $f_m \neq 0$ are present *only* in the parts of section Ω_2 (the graphite crucible)

which are labelled “uniform heat sources” in the left-hand part of Fig. 3. These parts satisfy $5.4\text{cm} \leq r \leq 6.6\text{cm}$ and $9.3\text{cm} \leq z \leq 42.0\text{cm}$. In that region, f_2 is set to the constant value $f_2 = 1.23\text{MW}/\text{m}^3$, which corresponds to a total heating power of 1.8 kW. This serves as an approximation to the situation typically found in a radio frequency induction-heated apparatus, where a moderate skin effect concentrates the heat sources within a few millimeters of the conductor’s outer surface.

Here, our main goal is to illustrate the effectiveness of our finite-volume scheme for computing the temperature field in a realistic complex geometry involving materials with anisotropic thermal conductivity. If the anisotropy in the thermal conductivity of the insulation is sufficiently large, we expect the isotherms to be almost parallel to the direction with the larger anisotropy coefficient. Because the use of a Dirichlet boundary condition (6.27a) can suppress such an alignment of the isotherms, we prefer the Robin condition (6.27b) on all of $\partial\Omega$. For $m \in \{1, 2, 6\}$, we set $\theta_{\text{ext},m} = 500\text{K}$ and $\zeta_m = 80\text{W}/(\text{m}^2\text{K})$.

We now present results of numerical experiments, varying the anisotropy coefficients (α_r^1, α_z^1) in the insulation. In each case, we use a fine grid consisting of 61222 triangles. We start with the isotropic case $(\alpha_r^1, \alpha_z^1) = (1, 1)$ depicted on the right-hand side of Fig. 3. In Fig. 4, we present the simulated temperature fields for the moderately anisotropic cases, where the anisotropy coefficients are given as $(\alpha_r^1, \alpha_z^1) = (10, 1)$ in the left figure, $(\alpha_r^1, \alpha_z^1) = (1, 10)$ in the middle figure and in the right figure, we have $(\alpha_r^1, \alpha_z^1) = (10, 1)$ in top and bottom insulation parts and $(\alpha_r^1, \alpha_z^1) = (1, 10)$ in insulation side walls.

The maximum temperatures established in the seven experiments are collected in Table 3.

Table 3: Maximum temperatures for numerical experiments, depending on the anisotropy coefficients (α_r^1, α_z^1) of the insulation (cf. Figs. 3 and 4).

α_r^1	α_z^1	maximal temperature [K]
1	1	1273.18
1	10	1232.15
1-10, mixed	1-10, mixed	1238.38
10	1	918.35

Comparing the temperature fields in Figs. 3 and 4 as well as the maximum temperatures listed in Table 3, we find that any anisotropy reduces the effectiveness of the thermal insulation. The stronger the anisotropy the less effective the insulation and any value above unity improves the insulation’s thermal conductivity in that direction. Similarly, when reducing one of the anisotropy coefficients to a value below unity, a stronger anisotropy would result in improved insulation.

The application of decoupling methods in this real-life application is very important, because of the complicated domains with different parameters. Each simpler domain can be computed more accurately and parallel computation is possible. In these presented examples, we only apply the decomposition methods for the test examples.

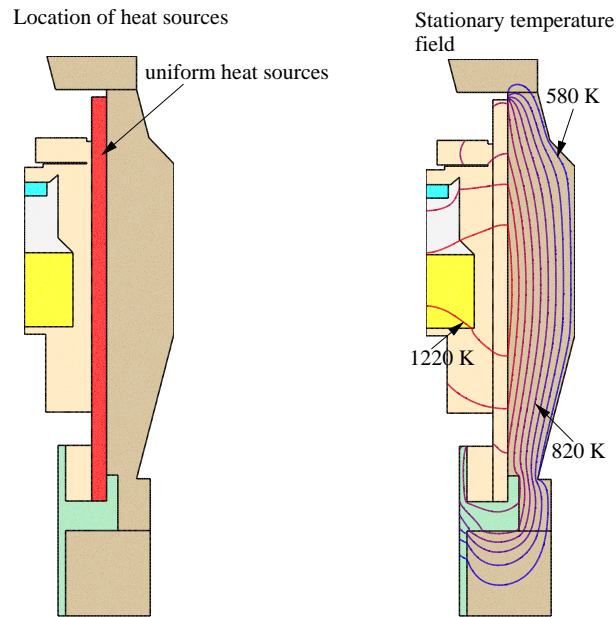


Figure 3: Left: location of the heat sources. Right: computed temperature field for the isotropic case $\alpha_r^1 = \alpha_z^1 = 1$, where the isotherms are spaced at 80 K.

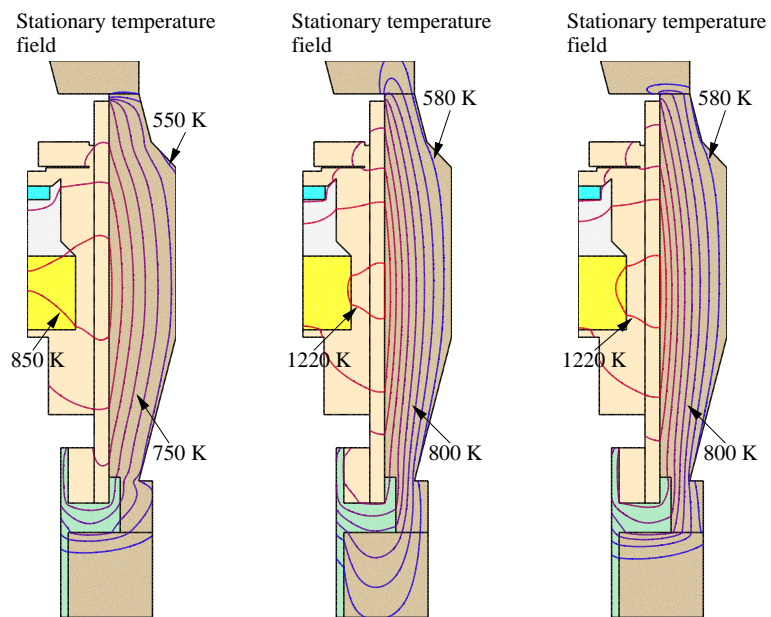


Figure 4: Computed temperature fields for the moderately anisotropic cases. Left figure, we deal with $(\alpha_r^1, \alpha_z^1) = (10, 1)$ and isotherms spaced at 50 K. Middle figure, we deal with $(\alpha_r^1, \alpha_z^1) = (1, 10)$ and isotherms spaced at 80 K. Right figure, we deal with $(\alpha_r^1, \alpha_z^1) = (10, 1)$ in top and bottom insulation parts, $(\alpha_r^1, \alpha_z^1) = (1, 10)$ in insulation side wall and isotherms spaced at 80 K.

The underlying real-life application can be computed more efficient using spatial decomposition methods. In subsequent experiments we will show that spatial decomposition methods are more adaptive to the underlying domains and can benefit from parallelization.

Remark 6.3. We discussed a complex model which can be decoupled using temporal and spatial decomposition methods, as proposed in the previous test examples, into smaller parts. These smaller models can be calculated with more efficient methods using less computational time. Because of this simplification to partial models, complicated models may be computed using more standard and less time-consuming methods. The coupling of such partial models can be done with iterative decomposition methods, which are optimal and quickly implemented.

7 Conclusion

The paper presents computations of a complex model of a crystal growth apparatus. Based on a complicated model equation, we decouple into simpler sub-problems in both time and space. These simpler sub-problems are solved by decomposition methods in time and space. We described a temporal and spatial splitting method of high order that decreases the splitting error enormously. Because of these new methods, the application of decomposition methods for time and space is more useful. The theoretical results are verified with numerical experiments and lastly we present a real-life problem, see [18]. One future direction for the decomposition method would be to understand the physical decoupling and apply the method to non-smooth and discontinuous problems. A second future development would be to recode standard software packages for one specific application and to couple them with decomposition methods using other standard software. Both future works aim to reduce the complexity of a given model and solve it with optimal iterative decomposition methods.

References

- [1] I. Aavatsmark, T. Barkve, Ø. Bøe and T. Mannseth, Discretisation on unstructured grids for inhomogeneous, anisotropic media. Part I: Derivation of the methods, *SIAM J. Sci. Comput.*, 19(5) (1998), 1700-1716.
- [2] I. Aavatsmark, T. Barkve, Ø. Bøe and T. Mannseth, Discretisation on unstructured grids for inhomogeneous, anisotropic media. Part II: Discussion and numerical results, *SIAM J. Sci. Comput.*, 19(5) (1998), 1717-1736.
- [3] I. Alonso-Mallo, B. Cano and J. C. Jorge, Spectral-fractional step Runge-Kutta discretisations for initial boundary value problems with time dependent boundary conditions, *Math. Comput.*, 73(248) (2004), 1801-1825.
- [4] J. Baranger, J. F. Maitre and F. Oudin, Connection between finite volume and mixed finite element methods, *Math. Model. Numer. Anal.*, 30(4) (1996), 335-465.
- [5] J. Bey, *Finite-Volumen- und Mehrgitterverfahren für elliptische Randwertprobleme*, B. G. Teubner, Stuttgart, Leipzig, Germany, 1998 (in German).

- [6] I. Braianov and L. Volkov, Numerical solution of a reaction-diffusion elliptic interface problem with strong anisotropy, *Computing*, 71 (2003), 153-173.
- [7] J. C. Butcher, *Numerical Methods for Ordinary Differential Equations*, John Wiley & Sons Ltd, Chichester, 2003.
- [8] Z. Chen, R. Li and A. Zhou, A note on the optimal L^2 -estimate of the finite volume element method, *Adv. Comput. Math.*, 16 (2002), 291-303.
- [9] P. G. Ciarlet and J. L. Lions (eds), *Finite Element Methods (Part 1). Handbook of Numerical Analysis, Vol. II*, North-Holland/Elsevier, Amsterdam, The Netherlands, 1991.
- [10] D. Daoud and J. Geiser, Overlapping Schwarz wave form relaxation for the solution of coupled and decoupled system of convection diffusion reaction equation, *Appl. Math. Comput.*, 190(1) (2007), 946-964.
- [11] F. Dupret, P. Nicodéme, Y. Ryckmans, P. Wouters and M. J. Crochet, Global modelling of heat transfer in crystal growth furnaces, *Int. J. Heat Mass Transfer*, 33(9) (1990), 1849-1871.
- [12] R. Eymard, T. Gallouët and R. Herbin, Finite volume methods, in: P. G. Ciarlet and J. L. Lions (Eds.), *Solution of Equations in \mathbb{R}^n (Part 3); Techniques of Scientific Computing (Part 3)*. *Handbook of Numerical Analysis, Vol. VII*, North-Holland/Elsevier, Amsterdam, The Netherlands, 2000, pp. 713-1020.
- [13] I. Faïlle, A control volume method to solve an elliptic equation on a two-dimensional irregular mesh, *Comput. Method. Appl. Mech. Engrg.*, 100 (1992), 275-290.
- [14] I. Farago and J. Geiser, Iterative operator-splitting methods for linear problems, *Int. J. Comput. Sci.*, 1(1-3) (2005), 64-74.
- [15] J. Fuhrmann, T. Koprucki and H. Langmach, pdelib: An open modular tool box for the numerical solution of partial differential equations. Design patterns, in: W. Hackbusch and G. Wittum (Eds.), *Proceedings of the 14th GAMM Seminar on Concepts of Numerical Software*, Kiel, January 23-25, 1998, University of Kiel, Germany, 2001.
- [16] J. Fuhrmann and H. Langmach, Stability and existence of solutions of time-implicit finite volume schemes for viscous nonlinear conservation laws, *Appl. Numer. Math.*, 37(1-2) (2001), 201-230.
- [17] V. F. Formalev, Heat and mass transfer in anisotropic bodies, *High Temperature*, 39(5) (2001), 753-774.
- [18] J. Geiser, O. Klein and P. Philip, Numerical simulation of heat transfer in materials with anisotropic thermal conductivity: A finite volume scheme to handle complex geometries, Preprint No. 1033, Weierstrass Institute for Applied Analysis and Stochastics, Berlin, 2005.
- [19] J. Geiser, Discretisation methods with embedded analytical solutions for convection dominated transport in porous media, *Lecture Notes in Mathematics*, Springer, vol. 3401, 2005, pp. 288-295.
- [20] J. Geiser, Discretisation methods with embedded analytical solutions for convection-diffusion dispersion-reaction equations and applications, *Appl. Math. Comput.*, 190(1) (2007).
- [21] J. Geiser, Decomposition methods for partial differential equations: Theory and applications in multiphysics, Habilitation Thesis, Humboldt University of Berlin, Germany, reviewed, 2007.
- [22] J. Geiser and C. Kravvaritis, A Domain Decomposition Method Based on Iterative Operator Splitting Method, Preprint No. 06-22, Humboldt University of Berlin, Department of Mathematics, Germany, 2006.
- [23] W. H. Hundsdorfer and J. Verwer, *Numerical Solution Of Time-Dependent Advection-Diffusion-Reaction Equations*, Springer, Berlin, 2003.

- [24] J. Kanney, C. Miller and C. Kelley, Convergence of iterative split-operator approaches for approximating nonlinear reactive transport problems, *Adv. Water Resour.*, 26 (2003), 247-261.
- [25] O. Klein, P. Philip and J. Sprekels, Modeling and simulation of sublimation growth of SiC bulk single crystals, *Interface. Free Bound.*, 6 (2004), 295-314.
- [26] O. Klein and P. Philip, Transient numerical investigation of induction heating during sublimation growth of silicon carbide single crystals, *J. Cryst. Growth*, 247(1-2) (2003), 219-235.
- [27] O. Klein and P. Philip, Correct voltage distribution for axisymmetric sinusoidal modeling of induction heating with prescribed current, voltage, or power, *IEEE T. Mag.*, 38(3) (2002), 1519-1523.
- [28] O. Klein and P. Philip, Transient temperature phenomena during sublimation growth of silicon carbide single crystals, *J. Cryst. Growth*, 249(3-4) (2003), 514-522.
- [29] O. Klein and P. Philip, Transient conductive-radiative heat transfer: Discrete existence and uniqueness for a finite volume scheme, *Math. Mod. Meth. Appl. Sci.*, 15(2) (2005), 227-258.
- [30] O. Klein, P. Philip, J. Sprekels and K. Wilmański, Radiation- and convection-driven transient heat transfer during sublimation growth of silicon carbide single crystals, *J. Cryst. Growth*, 222(4) (2001), 832-851.
- [31] H. Klie, W. Bangerth, X. Gai, M. F. Wheeler, P. L. Stoffa, M. Sen, M. Parashar, U. Catalyurek, J. Saltz and T. Kurc, Models, methods and middleware for grid-enabled multiphysics oil reservoir management, *Eng. Comput.*, 22 (2006), 349-370.
- [32] D. Kröner, *Numerical Schemes for Conservation Laws*, Advances in Numerical Mathematics, Wiley Teubner, Chichester, UK, Stuttgart, Germany, 1997.
- [33] R. J. LeVeque, *Finite Volume Methods for Hyperbolic Problems*, Cambridge Texts in Applied Mathematics, Cambridge University Press, 2002.
- [34] St. G. Müller, R. C. Glass, H. M. Hobgood, V. F. Tsvetkov, M. Brady, D. Henshall, D. Malta, R. Singh, J. Palmour and C. H. Carter Jr, Progress in the industrial production of SiC substrate for semiconductor devices, *Mater. Sci. Eng.*, B80(1-3) (2002), 327-331.
- [35] C. V. Pao, *Nonlinear Parabolic and Elliptic Equation*, Plenum Press, New York, 1992.
- [36] M. Parashar, V. Matossian, W. Bangerth, H. Klie, B. Rutt, T. M. Kurc, U. V. Catalyurek, J. H. Saltz and M. F. Wheeler, Towards dynamic data-driven optimization of oil well placement, *International Conference on Computational Science*, 2 (2005), 656-663.
- [37] P. Philip, *Transient Numerical Simulation of Sublimation Growth of SiC Bulk Single Crystal. Modeling, Finite Volume Method, Results*, Report No. 22, Weierstrass-Institute for Applied Analysis and Stochastics, Berlin, 2003.
- [38] O. Schenk and K. Gärtner, Solving unsymmetric sparse systems of linear equations with PARDISO, *J. Future Generation Comput. Syst.*, 20(3) (2004), 475-487.
- [39] O. Schenk, K. Gärtner and W. Fichtner, Scalable parallel sparse factorization with left-strategy on shared memory multiprocessor, *BIT*, 40(1) (2000), 158-176.
- [40] K. Semmelroth, N. Schulze and G. Pensl, Growth of SiC polytypes by the physical vapour transport technique, *J. Phys.-Condes. Matter.*, 16 (2004), S1597-S1610.
- [41] J. R. Shewchuk, Triangle: Engineering a 2D quality mesh generator and delaunay triangulator, in: *First Workshop on Applied Computational Geometry (Philadelphia, Pennsylvania)*, ACM, 1996, pp. 124-133.
- [42] G. Strang, On the construction and comparison of difference schemes, *SIAM J. Numer. Anal.*, 5 (1968), 506-517.
- [43] J. G. Verwer and B. Sportisse, A note on operator splitting in a stiff linear case, MAS-R9830, 1998.